ALONG-THE-CHANNEL MODELING OF POLYMER-ELECTROLYTE FUEL CELLS

Michael R. Gerhardt, Lalit M. Pant, Adam Z. Weber
Energy Conversion Group, Lawrence Berkeley National Laboratory, Berkeley, CA USA
Corresponding author: Adam Z. Weber, e-mail: azweber@lbl.gov

REFERENCE NO
FCEL-12

Keywords:
Fuel cell, model, polymer electrolyte, transport

ABSTRACT

Cost and durability of polymer electrolyte fuel cells (PEFCs) remain the major obstacles in the way of their commercialization. Optimizing these devices for high current density with low catalyst loading can reduce the cost of PEFCs. Mathematical modeling is an ideal tool for illustrating the complex interplay of reactant and water transport, electrochemical performance, and heat generation in PEFCs. In this work, we develop a "1+2D" model, in which a 2D fuel cell sandwich model is successively stepped along a channel to simulate downstream effects without the computational cost associated with 3D models. We highlight similarities and differences in water and thermal management for proton exchange membrane and anion exchange membrane fuel cells.

1. INTRODUCTION

Polymer-electrolyte fuel cells (PEFCs) have the potential to revolutionize the way in which we use energy, particularly in the transportation sector, where zero-emissions fuel-cell buses and cars have become increasingly popular. However, optimizing reactant and water transport in PEFCs remains critical for improving performance and enabling wide-spread adoption[1]. Computational modeling of transport phenomena in PEFCs is an ideal tool for optimizing cell parameters.

In this work, we explore two classes of PEFCs: proton-exchange-membrane fuel cells (PEMFCs) and anion-exchange-membrane fuel cells (AEMFCs). Both classes of PEFCs convert reactant hydrogen and oxygen gases to water and electricity, but the oxidation and reduction half-reactions are balanced by protons (H^+) or hydroxide anions (OH^-) respectively:

$$2H_2 \rightarrow 4H^+ + 4e^-, \quad (1)$$
$$O_2 + 4H^+ + 4e^- \rightarrow 2H_2O, \quad (2)$$

for PEMFCs, and

$$2H_2 + 4OH^- \rightarrow 4H_2O + 4e^-, \quad (3)$$
$$O_2 + 2H_2O + 4e^- \rightarrow 4OH^-, \quad (4)$$

for AEMFCs. Water management is critical in both types of cells. Flooding of the cell must be avoided, since liquid water will significantly reduce reactant mass transport and accessible catalyst active area. This is balanced by the need for humidification and hydration by the ion-exchange membranes used in each cell motif. Equations (1-4) highlight the differences in water management between the two cases: in PEMFCs, water is produced at the cathode, whereas in AEMFCs, water is consumed at the cathode and produced at the anode. Furthermore, the water production rate per electron in AEMFCs is double that of PEMFCs, so flooding at the anode might occur more rapidly.

To explore the operational aspects, we utilize a previously developed 2D fuel cell model [2, 3] and iterate them along the channel to construct a "1+2D" model that captures downstream effects of humidification, heating, and reactant consumption. The 1+2D framework was extended from our previous 1+1D work [4, 5]. This approach allows for simulation of along-the-channel effects using a sophisticated 2D MEA model without the computational complexity and computation time required for a full 3D simulation. In this work, we use the 1+2D model to compare and contrast downstream effects of humidification and reactant consumption in PEM and AEM fuel cells.

2. MATHEMATICAL MODEL

To model along-the-channel effects, the channel is divided into multiple segments, and a 2D membrane-electrode assembly (MEA) model is used at each segment to model the local current flowing through that segment, as shown in Figure 1. The details of the 2D models for both the PEMFC [2] and AEMFC [3] have been previously published; key equations are summarized here.

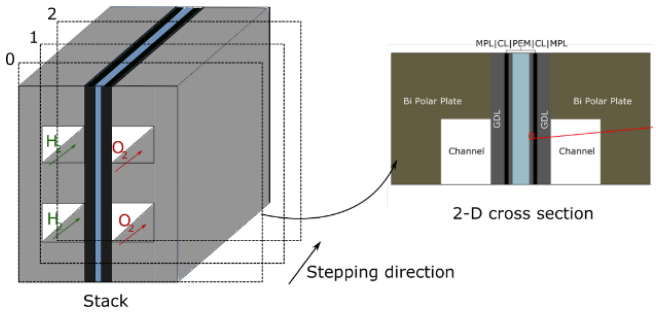

Fig. 1. Schematic of the 1+2D approach. (a) Full 3D stack with different cross-section steps along flow direction. (b) Schematic of 2D cross-section model.

Transport of ions and water are coupled by electro-osmosis, in which water is dragged along by flowing ions, and the streaming current, in which water movement down a chemical potential gradient induces a corresponding ion flux. These phenomena are described by Equations (5 and 6) [6]:

$$i = -\kappa \nabla \Phi - \frac{\kappa \xi}{F} \nabla \mu_0, \tag{5}$$

$$N_0 = -\frac{\kappa \xi}{F} \nabla \Phi - \left(\alpha + \frac{\kappa \xi}{F}\right) \nabla \mu_0, \tag{6}$$

where i is the ion current density, κ is the ionic conductivity, Φ is the electric potential, ξ is the electro-osmotic coefficient, F is Faraday's constant, μ_0 is the chemical potential of water, N_0 is the water flux, and α is the water transport coefficient. The membrane is assumed to have liquid-equilibrated and vapor-equilibrated values of $\alpha, \kappa,$ and ξ, as described in [6]. Two-phase flow of gases and liquid water is modelled by Darcy's law for each phase:

$$v_k = -\frac{K_k}{\mu_k} \nabla P_k, k \in l, g, \tag{7}$$

where v_k, K_k, μ_k, and P_k are the velocity, absolute permeability, viscosity, and pressure of phase k. Stefan-Maxwell diffusion is used to model diffusion of reactant gases:

$$J_i = -\rho_G \omega_i \sum_j^n \bar{D}_{ij} \left(\nabla x_j + \frac{(x_j - \omega_j)\nabla P_G}{P_G}\right) + \rho_G \omega_i v_G, \tag{8}$$

where J_i represents the mass flux of species i, ρ_G is the gas density, ω_i and x_i are the mass and molar fractions of species i, and $\bar{D}_{ij}$ is the inverted binary diffusion coefficient between species i and j.

2.1. Along-the-channel mass and heat balance

At each segment, consumption of reactant gases (hydrogen and oxygen) and production of water vapor are calculated and used in a mass balance along the channel to compute the species fluxes and concentrations entering the following segment:

$$N_{i,j+1} = N_{i,j} + L_{step} \iint S_i, \tag{9}$$

where $N_{i,j}$ is the molar flux of species i along the channel at step j, L_{step} is the length of the channel step (on the order of 5 mm), and S_i represents the molar sources and sinks of species i, integrated over either the anode or the cathode, which is obtained from the 2D fuel cell model. Gas concentrations for the next segment are computed from the fluxes:

$$x_{i,j+1} = \frac{N_{i,j+1}}{\sum_i N_{i,j+1}}, \tag{10}$$

and a heat balance determines the temperature of the segment:

$$h(T - T_c) = Q_{cell} + H_{in} \sum_i N_{i,j} - H_{out} \sum_i N_{i,j+1}, \tag{11}$$

where h is the heat transfer coefficient between the bipolar plate and the coolant

(typically about 1 W cm^{-2} K^{-1}), T is the temperature of the segment, T_c is the temperature of the coolant, Q_{cell} is the sum of heat sources from the 2D model, including resistive heating, exothermic electrochemical reactions, evaporation, and condensation, and H_{in} and H_{out} are the enthalpies of the gas flowing into and out of the channel, respectively.

3. RESULTS AND DISCUSSION

3.1. PEMFC modeling

The 1+2D model developed in Section 2 was used to simulate a segmented H_2-air PEM fuel cell. From the local current-density distribution in Figure 2a, it can be seen that there is a large difference in performance from cell inlet to cell outlet, with a maximum in current density occurring about two-thirds of the way along the channel. The increase in current density along the channel is caused in part by membrane hydration (Figure 2b). Water produced by the cell in one segment hydrates the membrane further downstream, resulting in increased ionic conductivity. The temperature increases due to cell inefficiencies as well as water condensation, thereby also altering the local relative humidity. The increase in conductivity is offset by increasing mass-transport losses due to the consumption of reactants and flooding within the porous media at high relative humidity, resulting in a decrease in current density near the cell outlet despite full humidification. These limitations could be overcome with adjustments to the pressure and flow rate, for example, or with flow-field engineering to improve mass transport as discussed in Section 3.3.

3.2. Anion exchange membrane modeling

AEMFCs exhibit a different set of challenges related to thermal and water management. The properties of AEMs tend to be more dependent on humidity than PEMs, resulting in increased sensitivity to relative humidity in operating AEMFCs [7]. Additionally, as noted above, water is consumed by the oxygen reduction reaction at the cathode, and produced by the hydrogen oxidation reaction at the anode. These effects impact the current distribution (Figure 3a) and relative humidity (Figure 3b)

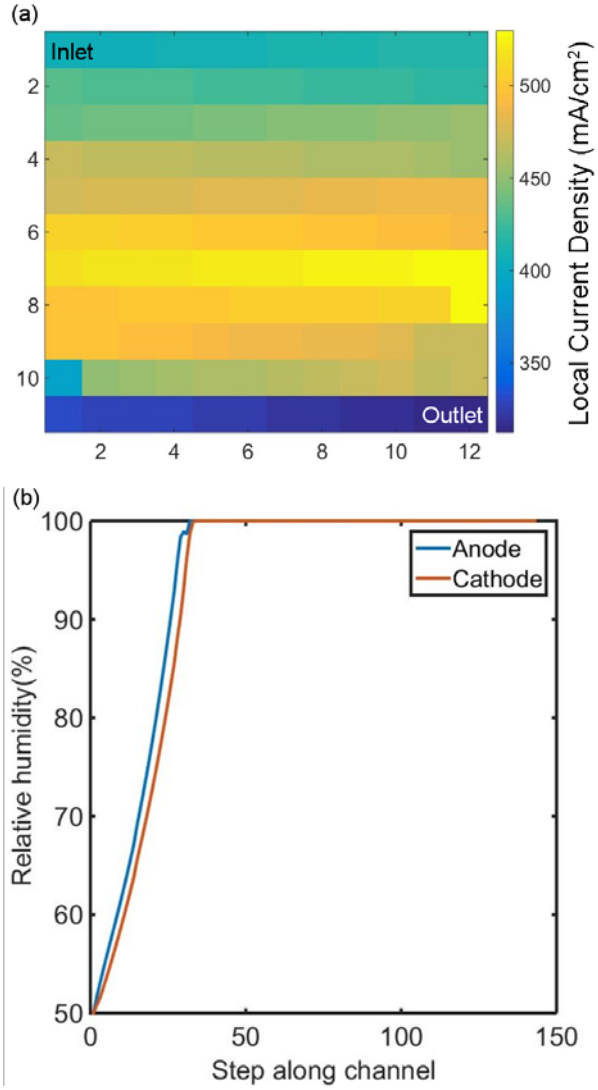

Fig. 2. Along-the-channel model for a H_2-air proton exchange membrane fuel cell. The operating temperature was 60 °C and inlet pressure was 150 kPa. The applied potential was 0.707 V. Flow rates were 1.5x stoichiometric flow for the anode and 2x stoichiometric flow for the cathode. (a) Local current density distribution illustrates a maximum when the membrane becomes fully hydrated. (b) Water produced from electrochemical reactions disperses through the MEA to humidify the anode and cathode inlets.

along the channel in the AEM fuel cell. The anode floods rather quickly (even with a pure hydrogen feed), resulting in a sharp drop in performance at the point the anode reaches full humidification. In contrast, the cathode is never fully humidified, although enough water

diffuses across the membrane to raise gradually the cathode relative humidity. By using pure oxygen instead of air, consumption of oxygen gas is negligible, and cell performance remains flat after the flooding event.

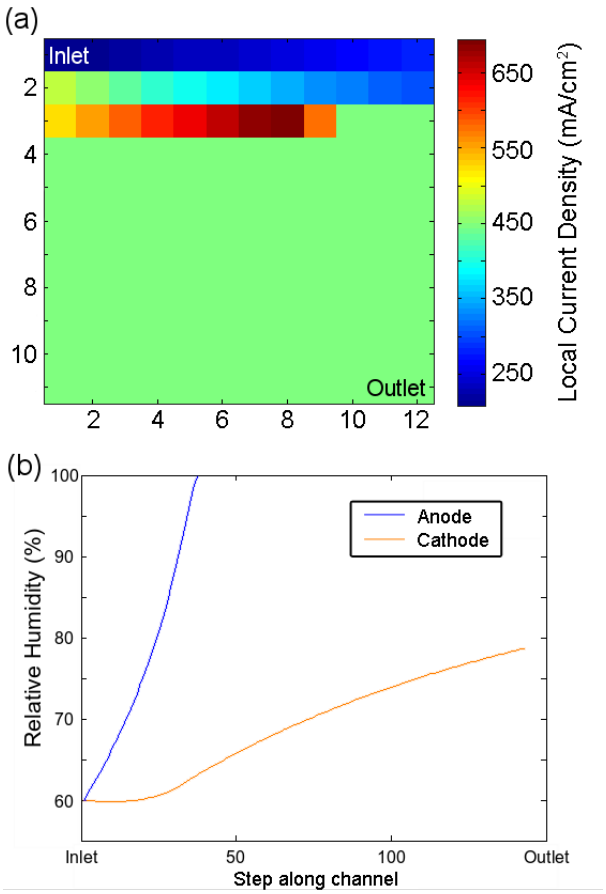

Fig. 3. (a) Local current density distribution and (b) relative humidity of anode and cathode gases along the channel for an H_2-O_2 anion exchange membrane fuel cell. The operating temperature was 60 °C, inlet pressure was 150 kPa. Flow rates were 2.8x stoichiometric flow for the cathode and 1.4x stoichiometric flow for the anode.

One challenge unique to AEMFCs is that carbon dioxide gas can react with hydroxide in the membrane to form carbonate and bicarbonate ions. The carbonate and bicarbonate ions reduce membrane conductivity and may impact reaction kinetics as well [8]. Including these effects in the 1+2D AEMFC model allows for computation of carbon dioxide concentration in the cathode and anode gas streams as a function of position down the channel, as shown in Figure 4 for an H_2-air AEMFC with 400 ppm CO_2 in the cathode feed. These results indicate significant concentration of CO_2 in the anode stream and highlight the critical need for further study of the downstream effects of CO_2 contamination in the anode gas.

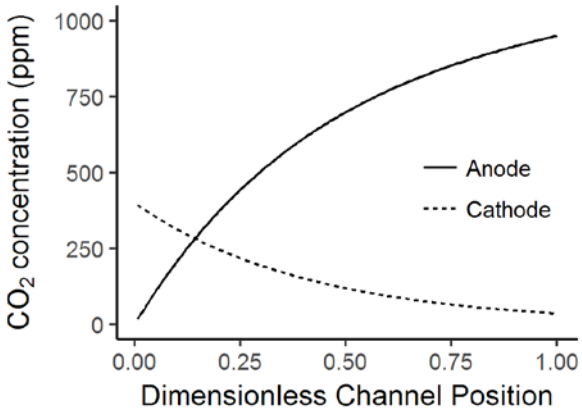

Fig. 4. Carbon dioxide concentration in the anode and cathode gas streams as predicted by an H_2-air AEMFC 1+2D model. The cell temperature was 60 °C and pressure was 120 kPa. The operating voltage was kept at 0.7 V, which caused a significant reduction in current density upon introduction of CO_2; hence the flow rates for both gases are 9x stoichiometric flow.

3.3. Effects of bends in serpentine flow fields

The results in the previous sections assume a single, straight channel for simplicity. Typically, fuel cells use serpentine flow fields, with channels that wind back and forth across the active area. At the bend point in the serpentine flow field, the wall blockage not only changes the direction of the gas stream, but also increases the amount of gas flow into the MEA sandwich (i.e., transport under the rib/land), causing higher local convection. To account for this increase in gas convection in the model, one can add an increment to the total gas pressure at the GDL/gas channel interface near each turning point. As shown in Figure 5, doing such a change by increasing the gas pressure by 10% at the turn points enables the model and experiments to come into agreement. As shown, the model can now predict the observed oscillations in local current density (Figure 5a) using a segmented cell hardware. This approach captures the observed performance changes with hardly

any additional model complexity and no effect on computation time.

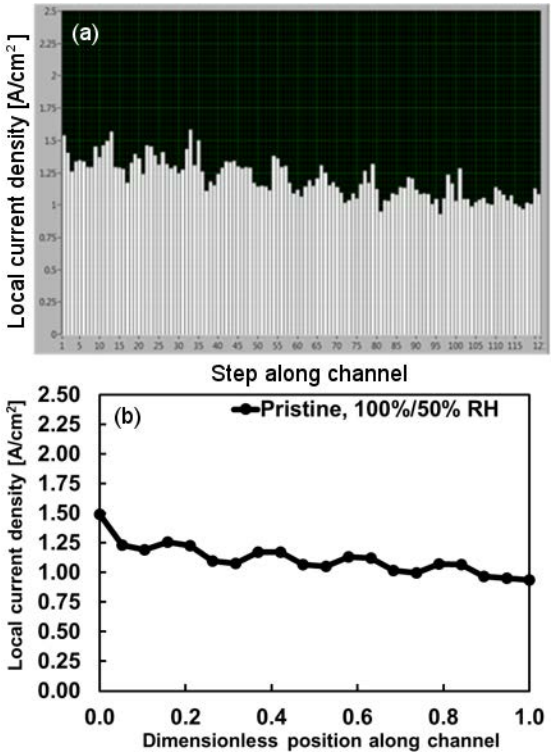

Fig. 5. (a) Experimental measurement and (b) model of local current density along a serpentine channel in a proton exchange membrane fuel cell. The oscillations in local current observed in (a) are due to increased convection at the bends in the serpentine flow field. These oscillations are modelled in (b) by increasing the gas pressure locally.

3. CONCLUSIONS

An along-the-channel model was presented that allows for prediction of local changes occurring downstream including humidity, concentrations, temperature, etc. These changes result in different local current densities, which can be compared to segmented cell data with good agreement. The model was also applied to proton- and anion-exchange-membrane fuel cells to compare and contrast issues in water management. It was shown how anion-exchange-membrane fuel cells have a much more nuanced and complex water management with more severe flooding and hydration requirements. Furthermore, the impact of carbon dioxide on anion-exchange-membrane fuel cells was also elucidated.

Acknowledgements

This work was funded by the Fuel Cell Technologies Office (FCTO), Office of Energy Efficiency and Renewable Energy (EERE), of the U.S. Department of Energy under contract number DE-AC02-05CH11231. We thank Iryna Zenyuk and Huai-Suen Shiau for helpful discussions and model development. We thank Julie Fornaciari for assistance with manuscript editing.

Nomenclature

$\overline{D}_{ij}$	Stefan-Maxwell binary diffusion coefficient between species i and j (cm^2/s)
F	Faraday's constant (C/mol)
H	Enthalpy of inlet/outlet fluid (J/mol)
h	Heat transfer coefficient ($W\ m^{-2}\ K^{-1}$)
i	Current density (A/cm^2)
J_i	Mass flux of species i ($kg\ m^{-2}\ s^{-1}$)
K_k	Permeability of phase k (m^2)
L_{step}	Length of step down channel
N_0	Water flux ($mol\ cm^{-2}\ s^{-1}$)
P_k	Pressure of phase k (Pa)
Q_{cell}	Sum of heat sources within cell (W/m^2)
S_i	Source term for species i
T	Temperature (K)
v_k	Velocity of phase k (m/s)
x_i	Mole fraction of species i

Greek Letters

α	Water transport coefficient ($mol^2\ J^{-1}\ cm^{-1}\ s^{-1}$)
κ	Ionic conductivity (S/cm)
μ_0	Water chemical potential (J/mol)
ξ	Electro-osmotic coefficient
Φ	Electric potential (V)

References

[1] A. Z. Weber *et al.*, "A Critical Review of Modeling Transport Phenomena in Polymer-Electrolyte Fuel Cells," *Journal of the Electrochemical Society*, vol. 161, no. 12, pp. F1254--F1299, 2014.

[2] I. V. Zenyuk, P. K. Das, and A. Z. Weber, "Understanding Impacts of Catalyst-Layer Thickness on Fuel-Cell Performance via Mathematical Modeling," *Journal of The*

Electrochemical Society, vol. 163, no. 7, pp. F691--F703, 2016.

[3] H.-S. Shiau, I. V. Zenyuk, and A. Z. Weber, "Elucidating Performance Limitations in Alkaline-Exchange-Membrane Fuel Cells," *Journal of The Electrochemical Society*, vol. 164, no. 11, pp. E3583--E3591, 2017.

[4] A. Z. Weber and J. Newman, "Coupled Thermal and Water Management in Polymer Electrolyte Fuel Cells," *Journal of The Electrochemical Society*, vol. 153, p. A2205, 2006.

[5] A. Z. Weber, "Gas-Crossover and Membrane-Pinhole Effects in Polymer-Electrolyte Fuel Cells," *Journal of The Electrochemical Society*, vol. 155, p. B521, 2008.

[6] A. Z. Weber and J. Newman, "Transport in Polymer-Electrolyte Membranes II. Mathematical Model," *Journal of The Electrochemical Society*, vol. 151, no. 2, p. A311, 2004.

[7] J. R. Varcoe *et al.*, "Anion-exchange membranes in electrochemical energy systems," *Energy & Environmental Science*, vol. 7, pp. 3135-3191, 2014.

[8] M. INABA *et al.*, "Effects of Carbon Dioxide on the Performance of Anion-Exchange Membrane Fuel Cells," *Electrochemistry*, vol. 79, pp. 322-325, 2011.